Heliyon 6 (2020) e04113

Contents lists available at ScienceDirect

Heliyon

journal homepage: www.cell.com/heliyon

Research article

Exploration of synthesized quaternary ammonium ionic liquids as unharmful anti-corrosives for aluminium utilizing hydrochloric acid medium

Tshimangadzo Nesane, Simon S. Mnyakeni-Moleele, Lutendo C. Murulana *

Department of Chemistry, School of Mathematical and Natural Sciences, University of Venda, Private Bag X5050, Thohoyandou 0950, South Africa

ARTICLE INFO

Keywords:
Materials chemistry
Physical chemistry
Aluminium
BOPAMS
BOBAMS
Spectroscopic methods
Electrochemical techniques

ABSTRACT

1-(benzyloxy)-1-oxopropan-2-aminium 4-methylbenzenesulfonate (BOPAMS) and 4-(benzyloxy)-4-oxobutan-1-aminium 4-methylbenzenesulfonate (BOBAMS) were prepared and confirmed through spectroscopic methods (FT-Infrared, Carbon 13-NMR and Proton-NMR). BOPAMS and BOBAMS were evaluated as unharmful inhibitors for aluminium corrosion. The anti-corrosive properties, inhibition mechanism, inhibitor-metal adsorption behaviour and corrosion inhibition efficiency were evaluated by employing approaches like gravimetric, potentiodynamic polarization (PDP) and electrochemical impedance spectroscopy (EIS). FT-IR demonstrated functional groups that are responsible for the binding of BOPAMS and BOBAMS with surfaces of aluminium. BOPAMS and BOBAMS resemble a semi-chemisorption/physisorption mechanism, obeying Langmuir binding model. The mechanism of binding adopted by BOPAMS and BOBAMS was proposed.

1. Introduction

Aluminium (Al) is a highly reactive metal that withstands most corrosive environments, although it can undergo corrosion if exposed directly to an aggressive environment. The corrosion resistance of Al is owed to the Al oxide film inert and protective nature, which forms on the metal surface when exposed to moisture (Abdulwahab et al., 2016; Kciuk et al., 2010; Kciuk and Tkaczyk, 2007; Shalabi et al., 2015). Aggressive acid solutions like hydrochloric acid (HCl) are extensively used in industries during the manufacturing of metallic equipments and in other applications such as acid pickling (Verma et al., 2020). During the pickling process, HCl leads to the corrosion of metal vessels and industrial pipelines, thereby reducing the production and resulting in the economic loss (Uhlig and King, 1972; Govindasamy and Ayappan, 2015). To circumvent the corrosion initiated by HCl, corrosion inhibitors are utilized. The utilization of corrosion inhibitors is regarded as an effective method towards the protection of materials from the wrath of corrosion in aggressive environments (Kim et al., 2006; Subasri et al., 2005). Substances that are utilized to protect materials from attack by aggressive species must possess properties that allow them to bind onto the surface of the material and slow down the dissolution of materials. The resultant barrier of chemisorbed substance protects the material by either delaying the electrochemical mechanism or by the role of demarcation between the material and the corrosive medium (Umoren, 2009). Most corrosion inhibitors that are utilized in solvent heating processes are harmful and non-biodegradable, which is a problem because it can lead to the emission of industrial wastewaters with a vast amount of toxic materials finding their path into waterways. Due to their toxicity, most inhibitor compounds do not meet entirely the required environmental protection standards (Antonijevic and Petrovic, 2008). Nowadays, many studies have been devoted to finding eco-friendly organic corrosion inhibitors. Ionic liquids (ILs) have enjoyed more employment as corrosion inhibitors to solve the toxicity problem. ILs resemble the nature of organic salts at atmospheric temperatures and their structures are composed of cations and anions (Zheng et al., 2014a,b). Recently Atta et al. reported on the use of quaternary ammonium salts, namely, Oleylammonium Tosylate and Octadecylammonium Tosylate (Atta et al., 2015). In their report, they concluded that these compounds work as effective semi-chemisorption/physisorption corrosion inhibitors when steel is exposed to diluted hydrochloric acid. Even though other ILs have demonstrated the ability to act as corrosion inhibitors for Al corrosion, no reports are describing the use of 1-(benzyloxy)-1-oxopropan-2-aminium 4-methylbenzenesulfonate (BOPAMS) and 4-(benzyloxy)-4-oxobutan-1-aminium 4-methylbenzenesulfonate (BOBAMS) as

* Corresponding author.
E-mail address: Lutendo.murulana@univen.ac.za (L.C. Murulana).

https://doi.org/10.1016/j.heliyon.2020.e04113
Received 3 April 2020; Received in revised form 11 May 2020; Accepted 28 May 2020

anticorrosives of Al utilizing hydrochloric acid medium. This paper reports on the continuation of the work that has been done in our research group in exploring the use of ILs as green inhibitors and adds more data to the literature already available. The most notable improvement or achievements characterizing the current work is the fact that the current ionic liquids were synthesized as opposed to being obtained from the commercially available ones. It is also paramount to note that these compounds are completely novel. The quaternary ammonium salts, namely BOPAMS and BOBAMS utilized as anticorrosives for Al corrosion in 1M hydrochloric acid in this present study are shown in Figure 1. Table 1 puts in comparison the corrosion inhibition abilities by various corrosion inhibitors that are reported in literature and the ones utilized in the current investigation.

2. Experimental

2.1. Materials

Al coupons composed of approximately 99 (wt %), were used as the working electrode for all experimental procedures performed in this study. The coupons had a dimension of 3 cm length × 2 cm breadth and contained a small hole of 2 mm diameter for hanging on a glass rod.

2.2. Preparations of solutions

Approximately 1M HCl aggressive solution was carefully made up through appropriate proportionating of 32% analytical grade HCl utilizing distilled H_2O. Parent solutions of 10.0×10^{-4} M BOPAMS and BOBAMS were thoroughly made up by weighing appropriate amounts of BOPAMS and BOBAMS, followed by the addition of distilled H_2O to the mark of 1000 cm^3 volumetric flasks. These parent solutions were utilized to make up various concentrations of BOPAMS and BOBAMS as reported in the results section of this paper.

2.3. Synthesis of BOPAMS and BOBAMS

The synthesis of ionic liquids followed reaction Scheme 1 below. The two compounds were synthesized by the suspension of alanine **1** (6.2124 g, 69.7395 mmol) and γ-amino butanoic acid **2** (7.0164 g, 68.0411 mmol) respectively with 10 cm^3 benzoyl alcohol **3** (10.4 g, 96.1716 mmol) in a mixture of p-toluenesulfonic acid monohydrate (PTSA) (14.5821 g, 84.6812 mmol) and toluene (200 cm^3). The mixture was stirred for 10 min and heated to reflux for 10 h with azeotropic removal of water. The two products were precipitated by the addition of Et_2O (100 cm^3), filtered, dissolved in CH_3OH (60 cm^3) and precipitated further by the addition of Et_2O (100 cm^3). After the filtration and drying, the products were obtained as white crystals. BOPAMS ($C_{17}H_{21}NO_5S$, Mol. Wt. 351,42), Yield: 25.3816 g, 91% and BOBAMS ($C_{18}H_{23}NO_5S$, Mol. Wt. 365,44), Yield: 23.0146 g, 93%. Spectral analysis was carried out to confirm the two ionic liquids.

2.4. Weight loss measurements

Al sheets were first weighed and then totally submerged in 100 cm^3 1M HCl without and with BOPAMS and BOBAMS at various molarities (1.0×10^{-4} M – 5.0×10^{-4} M) and temperatures (303–333K) for a period of 8 h. This procedure was performed in a temperature-controlled water bath for purposes of maintaining the heat during the submerging period. This was carefully followed by removing, cleaning with distilled H_2O and finally drying in open air. The overall weight change of the Al sheets was noted.

2.5. Electrochemical techniques

For the electrochemical experiments, a PGSTAT302N Autolab Potentiostat from Metrohm was utilized to carry out potentiodynamic polarization (PDP) as well as electrochemical impedance spectroscopy (EIS). This instrument was equipped with a three-electrode cell consisted of a saturated calomel (Ag/AgCl) reference electrode, Pt counter electrode and the Al sheet was utilized as the working electrode. For EIS, a bridge tube was used to place the working electrode near the reference electrode to minimize IR contribution/Ohmic trop from the electrolyte solution. During the PDP and EIS measurements, Al sheets were allowed to corrode in open circuit potential (OCP) freely for a period of 30 min. PDP studies were performed at –250 to +250 mV (SCE) and 1 mV s^{-1} potential and scan rate, respectively. EIS curves were done at 100 kHz–0.00001 kHz frequency range at OCP conditions through applying a signal amplitude perturbation of 5 mV by utilizing an AC indicator at corrosion potential. Al sheets that were utilized were of a 1 cm^2 total area in surface. Nyquist and Tafel curves were obtained from the EIS and PDP measurements, respectively.

3. Results and discussion

3.1. Characterization of BOBAMS and BOPAMS

The ^{1}H-NMR and ^{13}C-NMR spectra of BOBAMS and BOPAMS are represented in Figures 2 and 3, respectively. As expected the aromatic regions of the ^{1}H-NMR spectra of BOBAMS and BOPAMS are similar. The spectra are characterized by a broad singlet peak accounting for three protons at 8.36 ppm (BOPAMS) and 7.34 ppm (BOBAMS). Also, the two spectra contain two doublets each, which account for two protons each at 7.50 ppm and 7.13 ppm. Lastly, the aromatic region of the two spectra is characterized by a multiplet accounting for five protons at about 7.4 ppm. The heteroatomic and aliphatic regions of BOPAMS are characterized by a doublet accounting for three protons at 1.41 ppm, a singlet accounting for three protons at 3.41 ppm and another singlet accounting for two protons at 5.34 ppm. The same regions for BOBAMS are characterized by a quintet accounting for two protons at 1.81 ppm, a triplet accounting for two protons at 2.40 ppm, another triplet accounting for two protons at 2.62 ppm, a singlet accounting for three protons at 3.80 ppm and lastly a singlet accounting for two protons 5.11 ppm. The ^{13}C-NMR spectra represent the correct number of carbon atoms at the appropriate chemical shift values. A methyl carbon peak for BOBAMS was observed at around 21.24 ppm (CH3PTSA). Two methyl carbon peaks were observed at around 16.16 ppm (H3C(3)Aln) and 21.25 ppm (H3C(3)PTSA) for BOPAMS. There are four methylene carbon peaks at about 22.87 (CH2(3)GABA), 30.71 (CH2(2)GABA), 38.67 (CH2(4) GABA) and 66.07 (CH2Bn) ppm for BOBAMS. BOPAMS gave a methine carbon at approximately 31.16 ppm (HC(2)Aln) and a methylene carbon peak was observed at around 67.49 ppm (H2CBn). The aromatic protons of the benzene rings were found at around 125–128 ppm (CAr) and four

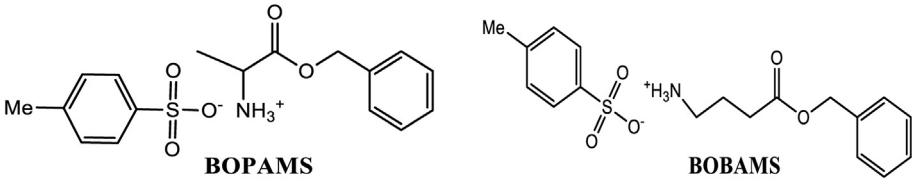

Figure 1. Molecular structures of BOPAMS and BOBAMS.

Table 1. Comparison of the corrosion inhibition abilities by various corrosion inhibitors that are reported in literature and the ones utilized in the current investigation.

Corrosion Inhibitor	Investigative Techniques	Adsorption mode	Aggressive medium/Metal	IE/%	Reference
2-hydroxyethyl trimethylammonium Chloride	Gravimetric, electrochemical, surface morphology, computational studies	Temkin adsorption isotherm, mixed-type inhibitors	1 M HCl/mild steel	92.04	Verma et al. (2018)
1-allyl-3-ethylimidazolium Bromide	Electrochemical, surface morphology, computational studies	Langmuir adsorption isotherm, chemisorption	0.5 M H_2SO_4/copper	92.5	Qiang et al. (2017)
3,3′-(1,4-phenylenebis(methylene)) bis(1-alkyl-1H-imidazol-3-ium) bromide	Electrochemical	Mixed-type inhibitors	0.5 M H_2SO_4/Stainless steel	90.7	Nessim et al. (2018)
1-butyl-1-methylpyrrolidinium trifluoromethyl sulfonate	Electrochemical, surface Morphology	Langmuir adsorption isotherm	3.5% NaCl/mild steel	91.4	El-Shamy et al. (2015)
Current ILs	Gravimetric, electrochemical, spectroscopic	Langmuir adsorption isotherm, mixed-type inhibitors	1 M HCl/aluminium	97.8	

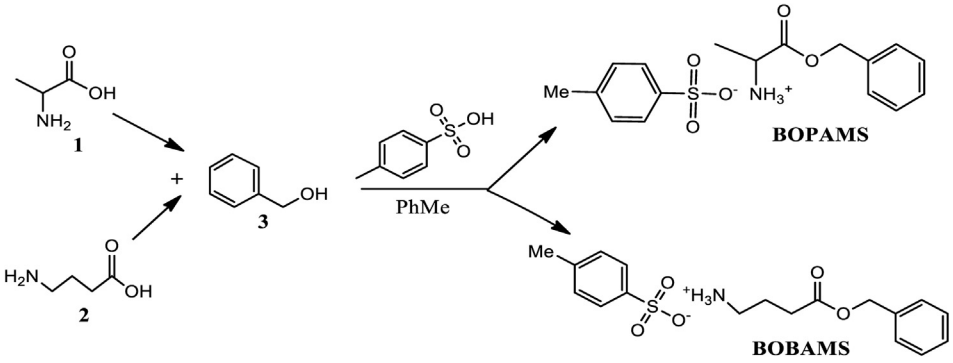

Scheme 1. Synthetic scheme of BOPAMS and BOBAMS.

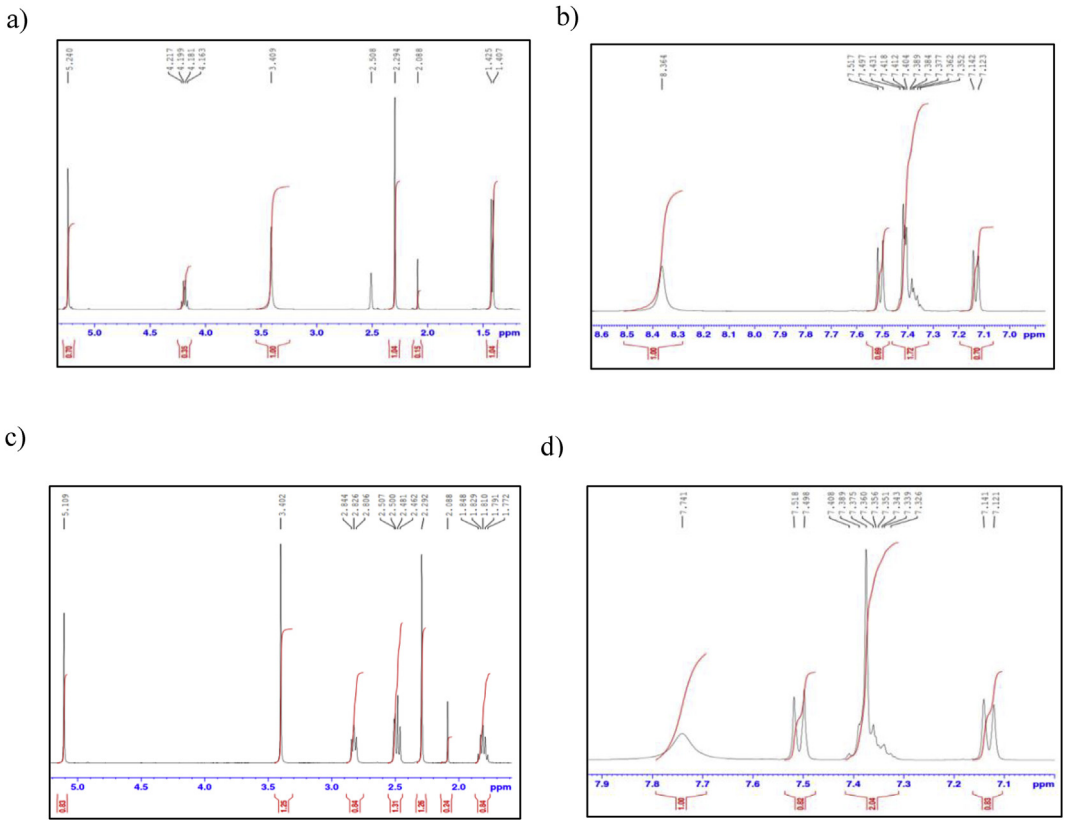

Figure 2. [1]H-NMR spectra a), b) BOPAMS and c), d) and BOBAMS.

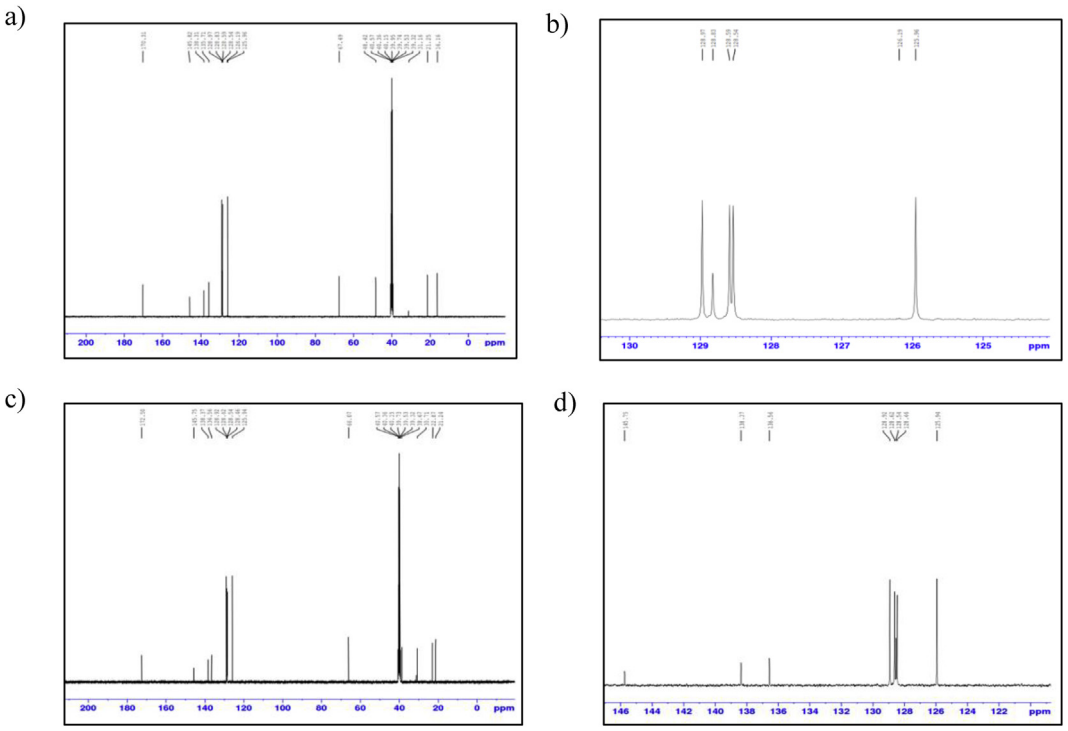

Figure 3. ^{13}C-NMR spectra a), b) BOPAMS and c), d) BOBAMS.

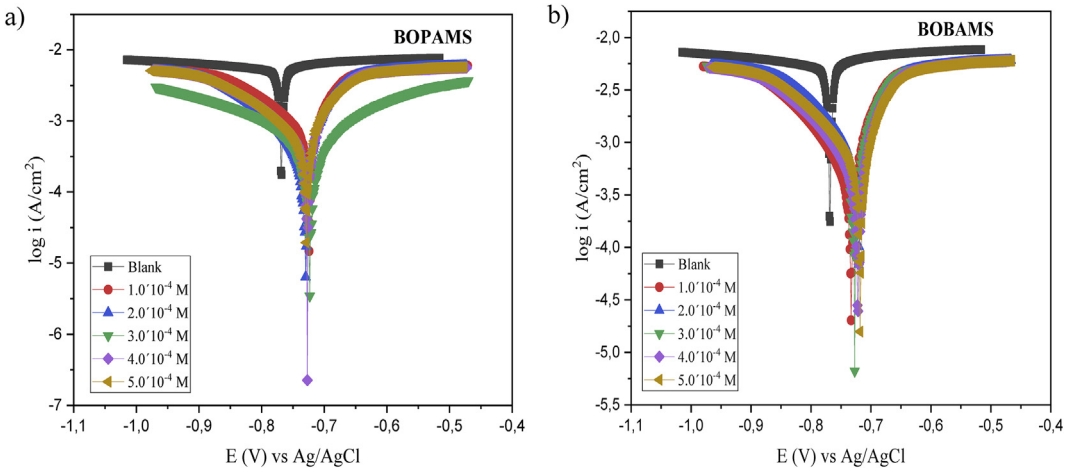

Figure 4. Tafel plots of Al utilizing 1M HCl for the process without and with of various molarities of a) BOPAMS and b) BOBAMS.

Table 2. PDP data of Al corrosion utilizing 1M HCl for the process without and with various molarities of BOPAMS and BOBAMS at 303K.

Inhibitor	Conc./M	E_{corr}/mV	i_{corr}/mAcm^{-2}	β_a/mVdec^{-1}	β_c/mVdec^{-1}	R_p (10^{-1})/Ω cm^2	IE/%
Blank	–	–769	0.00491	51	101	30.10	–
BOPAMS	1.0×10^{-4}	–724	0.00070	7	16	30.50	85.74
	2.0×10^{-4}	–730	0.00043	6	15	43.76	91.24
	3.0×10^{-4}	–723	0.00027	11	12	98.28	94.50
	4.0×10^{-4}	–727	0.00019	3	4	38.94	96.13
	5.0×10^{-4}	–729	0.00012	2	2	36.44	97.59
BOBAMS	1.0×10^{-4}	–723	0.00083	10	24	36.62	83.10
	2.0×10^{-4}	–721	0.00072	8	1	29.63	85.34
	3.0×10^{-4}	–727	0.00048	6	12	34.15	90.22
	4.0×10^{-4}	–722	0.00034	4	10	38.44	93.08
	5.0×10^{-4}	–718	0.00015	2	2	28.08	96.95

quintenary peaks at about 135, 138, 145, and 170 ppm (CO2Bn) for both BOBAMS and BOPAMS.

3.2. Potentiodynamic polarization (PDP)

Figure 4 shows the characteristic polarization plots found from the corrosion trait of Al in 1M HCl without and with of various concentrations of BOPAMS and BOBAMS at 303K. The values of different electrochemical parameters like corrosion current density (I_{corr}), corrosion potential (E_{corr}), anodic and cathodic Tafel slopes (β_a and β_c) were found by the manipulation of the oxidation and reduction current-potential up to their intersection, and their values are shown in Table 2. The potentiodynamic efficiencies (%IE_{PDP}) based on corrosion current density values were obtained utilizing Eq. (1) (Murulana et al., 2015).

$$IE_{PDP} = \left(\frac{i^0_{corr} - i^i_{corr}}{i^0_{corr}}\right) \times 100 \quad (1)$$

where i^0_{corr} and i^0_{corr} represent values of corrosion current density without and with BOPAMS and BOBAMS, respectively.

Tafel extrapolation plots show that the introduction of BOPAMS and BOBAMS altered both the oxidation and reduction sections and caused a decrease in the current densities relative to the ones observed in the blank. The decline is slightly pronounced with increases of BOPAMS and BOBAMS concentrations. The reduction effect, however, is somewhat more noticeable, indicating the process is predominantly of cathodic nature. This kind of behaviour of the BOPAMS and BOBAMS suggests that the acidic attack on the Al surface is hindered. In the reduction region, there is a rise to the parallel effect of the Tafel lines, signifying the activation control of the hydrogen evolution process. This effect indicates that the discharge of hydrogen occurs via the charge transfer process at the metal interface (Musa et al., 2010; Zheng et al., 2014a,b). Literature studies show that if the change in E_{corr} is higher than ±85 mV relative to that of the blank experiments, then BOPAMS and BOBAMS are said to be either oxidation or reduction inhibitors (Ghames et al., 2017). The highest change in the E_{corr} data from the present study were less than 85 mV with BOPAMS and BOBAMS. This kind of change confirms that neither BOPAMS nor BOBAMS are wholly oxidation or reduction but semi-chemisorption/physisorption inhibitors. The data presented in Table 2 shows that there is a change in the shift of both β_a and β_c compared to the blank experiments. The i_{corr} values lowered markedly with a rise in the concentration of BOPAMS and BOBAMS and the %IE_{PDP} congruently increased to a maximum at their highest concentrations. This observation by BOPAMS and BOBAMS suggests that they bind on the Al surface and the binding effect increases and become stable due to the availability of more BOPAMS and BOBAMS molecules at higher concentrations.

3.3. Electrochemical impedance spectroscopy (EIS)

The impendence spectra found for Al in 1M HCl solution at various concentrations of BOPAMS and BOBAMS are presented as Nyquist plots as indicated in Figure 5. EIS data found from these data are presented in Table 3. The shape of the curves is the same without or with BOPAMS and BOBAMS. This behaviour signifies that the presence of BOPAMS and BOBAMS does not alter the oxidation and reduction processes of the dissolution of Al. In some cases, there was a shift in Nyquist plots origin as the concentrations of BOPAMS and BOBAMS were raised. This behaviour can be theoretically accounted for by the formation of the binding film layer on the Al surface. Furthermore, as the concentration of BOPAMS and BOBAMS were amplified, more BOPAMS and BOBAMS molecules were able to provide higher coverage of the Al surface. This shift might also be as a consequence of the stabilization of the binding process and the reduction of the passivation of Al. The semicircles obtained are not perfect, and a smaller arch for the blank shows that the corrosion of Al is due mainly to the charge sharing process which also suggests that the Faradaic processes that occur on bare Al surface lower with the introduction of BOPAMS and BOBAMS. As such, BOPAMS and BOBAMS do not change the electrochemical process of corrosion but prevent it by binding on the metal surface (El-Azaly, 2019).

Nyquist diagram presented here consists of a capacitive loop in the high-frequency areas followed by an inductive loop in the low-frequency areas. The high-frequency capacitive loop is said to be a representative of the charge transfer resistance of the corrosion process and the double layer behaviour. The behaviour of the inductive loop may be a consequence of several phenomena. For instance, it can be accounted for as the relaxation of the substances present within the oxide layer covering the electrode surface. Furthermore, through the Ladha and Hachelef's measurements (Ladha et al., 2015; Hachelef et al., 2016), the inductive loop has been confirmed to be linked with the presence of the film on of passivation on Al. Moreover, another cause for the induction loop could be as a consequence of the stabilization of the binding intermediate complex on the electrode surface that might involve the reactive products as well as the molecules of the BOPAMS and BOBAMS (Ladha et al., 2015; Yurt et al., 2006). The relevant electrical circuit structure utilized to fit the impendence spectra has been reported previously (Yurt et al., 2006; Khaled and Al-Qahtani, 2009) and is shown in Figure 6. In this electrical circuit, R_1 represents the electrolyte resistance (R_s), Q_1 represents constant phase element (CPE), R_2 represents the charge transfer resistance (R_{ct}), and R_3 and L_3 represent the inductive elements. Constant phase element was utilized as opposed to double-layer capacitance (C_{dl}) to reflect a perfect capacitor in order to describe the inhomogeneities within the system. The imperfect semicircle loop at higher frequency section indicates the inhomogeneity of the Al surface due to structural or interfacial origin similar to those existing during the binding processes (Zheng

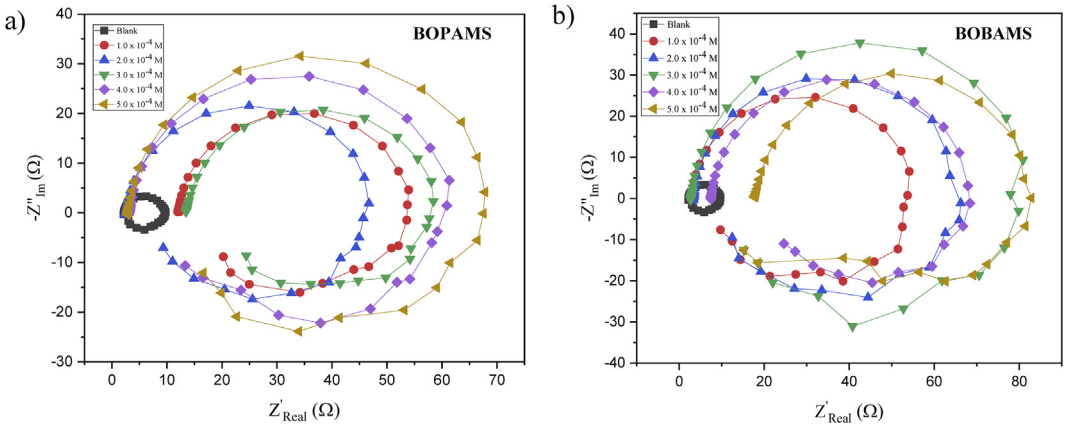

Figure 5. Nyquist plots of Al utilizing 1M HCl for the process without and with of various molarities of a) BOPAMS and b) BOBAMS.

Table 3. EIS data of Al corrosion utilizing 1M HCl for the process without and with various molarities of BOPAMS and BOBAMS at 303K.

Inhibitor	Conc./M	$^{Rct/}\Omega$	$Q_1/F.s^{(a-1)}$	R_s/Ω	R_3/Ω	N	L_3/H	Θ	IE/%
Blank	–	0.4036	0.1146e-3	2.200	6.873	0.9463	2.902	–	–
BOPAMS	1.0×10^{-4}	5.864	96.49e-6	12.09	34.85	0.9807	14.01	0.9312	93.12
	2.0×10^{-4}	6.019	83.83e-6	2.537	37.68	0.9611	11.39	0.9329	93.29
	3.0×10^{-4}	9.217	68.51e-6	13.57	34.33	0.9662	12.24	0.9562	95.62
	4.0×10^{-4}	9.410	82.29e-6	3.167	47.30	0.9629	16.29	0.9571	95.71
	5.0×10^{-4}	11.30	88.66e-6	2.961	52.81	0.9599	52.81	0.9643	96.43
BOBAMS	1.0×10^{-4}	6.342	61.16e-6	2.889	44.21	0.9678	11.61	0.9364	93.64
	2.0×10^{-4}	7.769	69.66e-6	3.380	53.32	0.9641	15.44	0.9480	94.80
	3.0×10^{-4}	11.52	68.73e-6	2.823	64.62	0.9629	17.80	0.9650	96.50
	4.0×10^{-4}	15.80	99.50e-6	7.467	44.38	0.9623	14.41	0.9745	97.45
	5.0×10^{-4}	18.71	83.55e-6	17.92	44.97	0.9559	18.11	0.9784	97.84

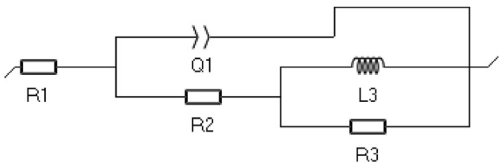

Figure 6. Relevant electrical circuit utilized to fit the impedance spectra obtained for Al corrosion in 1M HCl for the process without and with BOPAMS and BOBAMS.

et al., 2014a,b). Using Eq. (2) (Murulana et al., 2015), the inhibition efficiency (%IE_{EIS}) at different concentration of the inhibitors was calculated.

$$\%IE_{EIS} = \left(1 - \frac{R_{ct}^{0}}{R_{ct}}\right) \times 100 \quad (2)$$

where; R_{ct}° represents the charge transfer resistance without BOPAMS and BOBAMS and R_{ct} is the charge transfer resistance with BOPAMS and BOBAMS.

As shown in Table 3, it can be noticed that the %IE_{EIS} rises as the charge transfer resistance increases. Additionally, this rise is proportional to the rise of the concentration of BOPAMS and BOBAMS. The fall in the capacity as the BOPAMS and BOBAMS concentrations are raised can be due to the formation of the binding film layer by the BOPAMS and BOBAMS molecules on Al surface (Tsuru et al., 1978). The decrease can also be due to the rise in the thickness of the electrical double layer or the fall in local dielectric constant, indicating that the molecules of BOPAMS and BOBAMS work by binding at the interface between the solution and the Al surface through the displacement of water molecules (Alaoui et al., 2020).

3.4. Weight loss measurements

To further understand the mode of binding of BOPAMS and BOBAMS on Al surface and assess the impact of temperature on the corrosion process, weight loss measurements were studied. The consequence of temperature on the binding and calculation of activation parameters for Al corrosion was evaluated from the Arrhenius-type graph according to Eq. (3) (Murulana et al., 2015).

$$logC_R = logA - \frac{E_A}{2.303RT} \quad (3)$$

where E_a represents the apparent activation energy for the corrosion process which signifies the energy necessary for a molecule to react, C_R represents the corrosion rate in $g.cm^{-2}.h^{-1}$, A represents the Arrhenius pre-exponential factor, T represents the absolute temperature, and R represents the universal gas constant.

Table 4 shows that the %IE increases with an increase in the concentration of the two inhibitors studied. For instance, at 303K when the concentration of BOPAMS was 1.0×10^{-4} M the %IE was found to be 87.16 % and increased to a maximum of 93.52 % at 5.0×10^{-4} M. The same trend was observed in the case of BOBAMS wherein the obtained inhibition efficiency at 1.0×10^{-4} M was 89.74% and at 5.0×10^{-4} M was 91.94%. The increase in %IE with an increase in the concentrations of the inhibitors can be attributed to the accumulation of a greater number of molecules on the surface of Al as the inhibitor concentration is increased,

Table 4. Weight loss data of Al corrosion utilizing 1M HCl for the process without and with various molarities of BOPAMS and BOBAMS at various temperatures.

Inhibitor	Conc./M	303K IE		313K		323K		333K	
		$C_R/g.cm^{-2}.h^{-1}$	IE/%	$C_R/g.cm^{-2}.h^{-1}$	IE/%	$C_R/g.cm^{-2}$ h^{-1}	IE/%	$C_R/g.cm^{-2}.h^{-1}$	IE/%
Blank	–	0.0128	–	0.0150	–	0.0190	–	0.0186	-
BOPAMS	1.0×10^{-4}	0.00164	87.16	0.00470	68.62	0.00576	63.78	0.00821	63.16
	2.0×10^{-4}	0.00136	89.33	0.00377	74.79	0.00572	64.02	0.00679	63.56
	3.0×10^{-4}	0.00152	90.98	0.00313	79.09	0.00501	68.47	0.00676	63.70
	4.0×10^{-4}	0.00112	91.26	0.00306	80.72	0.00479	69.86	0.00675	63.75
	5.0×10^{-4}	0.00083	93.52	0.00225	84.93	0.00383	75.94	0.00673	63.86
BOBAMS	1.0×10^{-4}	0.00131 0.0015	89.74	0.00290	80.64	0.00460	69.30	0.00647	65.26
	2.0×10^{-4}	0.00115	91.00	0.00270	82.00	0.00457	69.47	0.00634	65.96
	3.0×10^{-4}	0.00112	91.21	0.00256	82.89	0.00393	73.78	0.00625	66.47
	4.0×10^{-4}	0.00109	91.44	0.00181	87.91	0.00374	75.00	0.00610	67.28
	5.0×10^{-4}	0.00103	91.94	0.00161	89.25	0.00352	77.84	0.00582	68.75

which lead to the separation of the Al surface from the acidic solution and retarding the dissolution of Al (Ezeoke et al., 2012).

From the straight-line type of graph of log C_R against 1/T (Figure 7), the numerical data of E_a for various concentrations of BOPAMS and BOBAMS were obtained utilizing the slopes and can be utilized to explain the inhibitive mechanism further. The results obtained from these graphs are shown in Table 4. Figure 7 shows the blank with flatter slope indicating that it has smaller activation energy. When BOPAMS and BOMAMS are introduced into the system, the slope is much steeper with higher activation energy. The similarity in the trend of these figures suggests that the two inhibitors have the same mechanism of action. The data of E_a attained from the figures without the presence of BOPAMS and BOBAMS was 9.9215 kJ mol^{-1}. However, evidently the E_a data when 1.0×10^{-4} M BOPAMS was added, increased instantly to 41.8773 kJ mol^{-1}. BOBAMS also revealed a similar trend of the increase in activation energy which rises immediately when the smallest concentration of the BOBAMS is introduced into the system. This rise signifies that in the availability of BOPAMS and BOMAMS the barrier of energy for the corrosion reaction is induced, and the magnitude of the rise is related to the concentration of BOPAMS and BOBAMS (El-Lateef et al., 2019).

Kinetic data like enthalpy (ΔH_a^*) and entropy (ΔS_a^*) of activation can be used to provide further details on the dependence of inhibition efficiencies of BOPAMS and BOMAMS on temperature and the concentration of the inhibitor. These data were determined using the equation of transition state (4) (Murulana et al., 2015):

$$log\left(\frac{C_R}{T}\right) = \left[log\left(\frac{R}{Nh}\right) + \left(\frac{\Delta S^*}{2.303R}\right)\right] + \left(\frac{-\Delta H^*}{2.303R}\right)\left(\frac{1}{T}\right) \quad (4)$$

where R represents the universal gas constant, h represents the Plank's constant, T represents the absolute temperature, 2.303 is a numerical value utilized to convert from ln to log and N represents the Avogadro's number.

The straight-line graph of log (C_R/T) against 1/T (Figure 8) has a slope equivalent to (–ΔH*/2.303R) and y-intercept equivalent to [log (R/Nh) + ΔS*/2.303R]. This information enabled the estimation of activation data (ΔH* and ΔS*) which are listed in Table 5. Some insight into a possible type of adsorption mode of BOPAMS and BOBAMS can be gained by relating the corrosion activation data without and with the synthesized compounds. (–) data of ΔS* indicate that the damage on the metal surface has decreased and the (+) data indicate that the chaosness of the process has risen. Large (–) data of ΔS* are indicative of association of the activated complex in the slowest elementary reaction as opposed to dissociation. This signifies that the destruction on the Al surface has been lessened during the process of migrating from reactants to the activated complex as a result of the binding of BOPAMS and BOBAMS molecules on the Al surface (Verma et al., 2015; El-Katori et al., 2020). (+) sign of ΔH* data of the results reflects that the binding of BOPAMS and BOBAMS molecules is of endothermic character. ΔH* data for the uninhibited solution was 7.3147 kJ mol^{-1} and increased to 39.2549 and 41.6667 kJ mol^{-1} after the addition of 1.0×10^{-4} M BOPAMS and BOBAMS, respectively. This indicates that significant amount of energy was required to form a corrosion product, indicating that the presence of BOPAMS and BOBAMS resulted in the difficulty for the dissolution of the Al surface which increased as the inhibitor concentrations were increased.

3.5. Adsorption isotherms and thermodynamic parameters

The binding of BOPAMS and BOBAMS on Al surface is a critical step in the corrosion inhibition mode, which can be explained by adsorption isotherms (Maayt and Al-Rawashdeh, 2004). Therefore, to ascertain the mode of adsorption for BOPAMS and BOBAMS, several well-known adsorption isotherms were adopted and among them, the optimum correlation was obtained through Langmuir adsorption isotherm, which was achieved through a graph of surface coverage (θ) against the concentrations of BOPAMS and BOBAMS. According to Langmuir, θ is related to the inhibitor concentration (C_{inh}) in the bulk of the solution as well as the adsorption constant (K_{ads}), according to Eq. (5) (Ekanem et al., 2010).

$$\frac{C_{inh}}{\theta} = \frac{1}{K_{ads}} + C_{inh} \quad (5)$$

Thermodynamic parameters provide information relating to the strength and inhibitive mechanism of corrosion by the inhibitor. The ΔG°_{ads} values were obtained from K_{ads} using Eq. (6) (Murulana et al., 2015).

$$\Delta G^\circ_{ads} = -RTln(55.5K_{ads}) \quad (6)$$

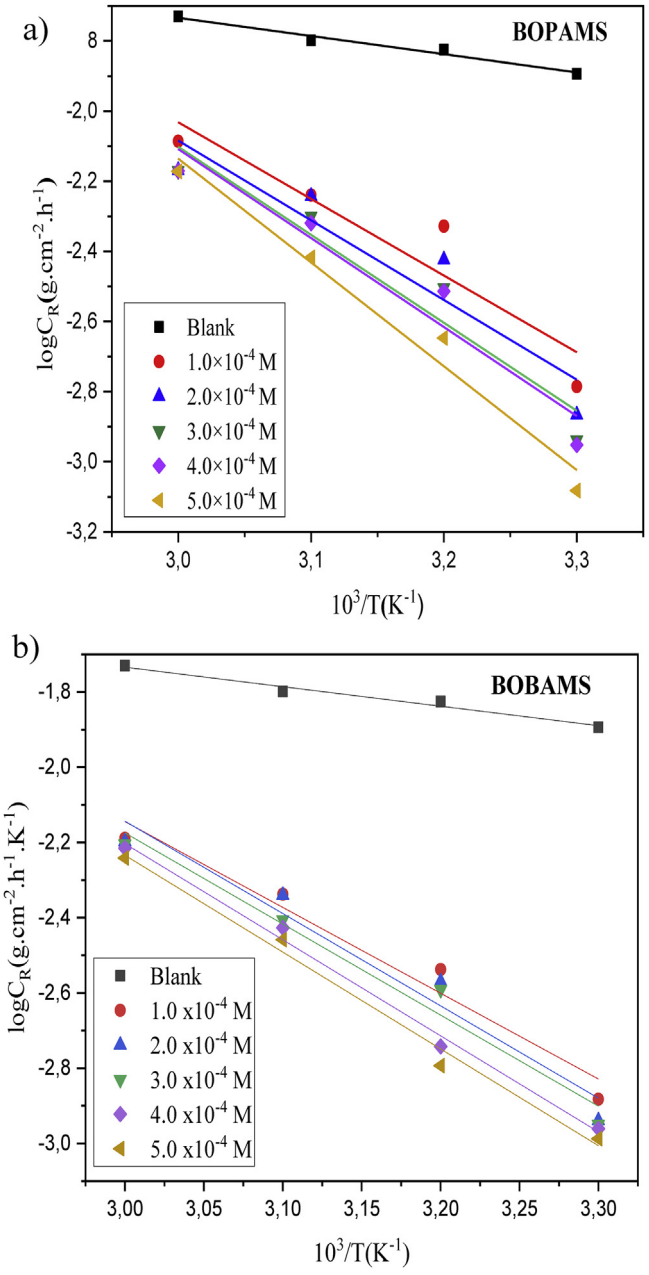

Figure 7. Arrhenius plots of Al utilizing 1M HCl for the process without and with of various molarities of a) BOPAMS and b) BOBAMS.

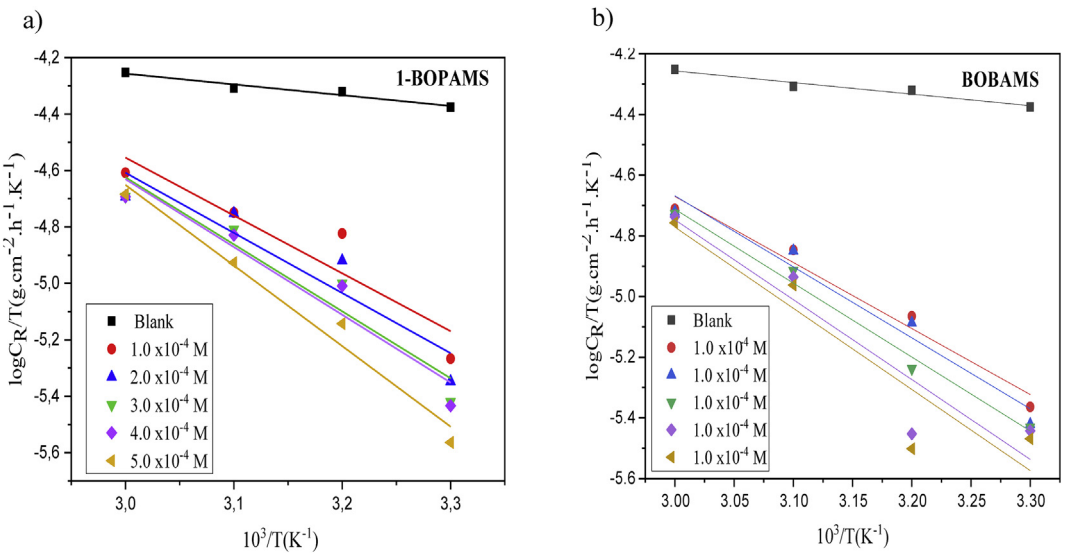

Figure 8. Transition state plots of Al utilizing 1M HCl for the process without and with of various molarities of a) BOPAMS and b) BOBAMS.

Table 5. Kinetic and activation data of Al corrosion utilizing 1M HCl for the process without and with various molarities of BOPAMS and BOBAMS.

Inhibitor	Conc./M	E_a/kJ.mol^{-1}	ΔH*/kJ.mol^{-1}	ΔS*/J.mol^{-1}·K^{-1}
Blank	–	9.9215	7.3147	-200.2395
BOPAMS	1.0 × 10^{-4}	41.8773	39.2549	-195.5330
	2.0 × 10^{-4}	43.5356	40.8088	-195.3432
	3.0 × 10^{-4}	48.0641	45.4519	-194.6320
	4.0 × 10^{-4}	48.6194	45.9999	-194.5527
	5.0 × 10^{-4}	56.7115	54.6709	-193.2145
BOBAMS	1.0 × 10^{-4}	43.6773	41.6667	-195.2710
	2.0 × 10^{-4}	46.9899	44.7879	-194.7799
	3.0 × 10^{-4}	46.3580	46.6452	-194.5330
	4.0 × 10^{-4}	48.8856	50.3792	-193.9810
	5.0 × 10^{-4}	49.7281	51.2025	-193.8779

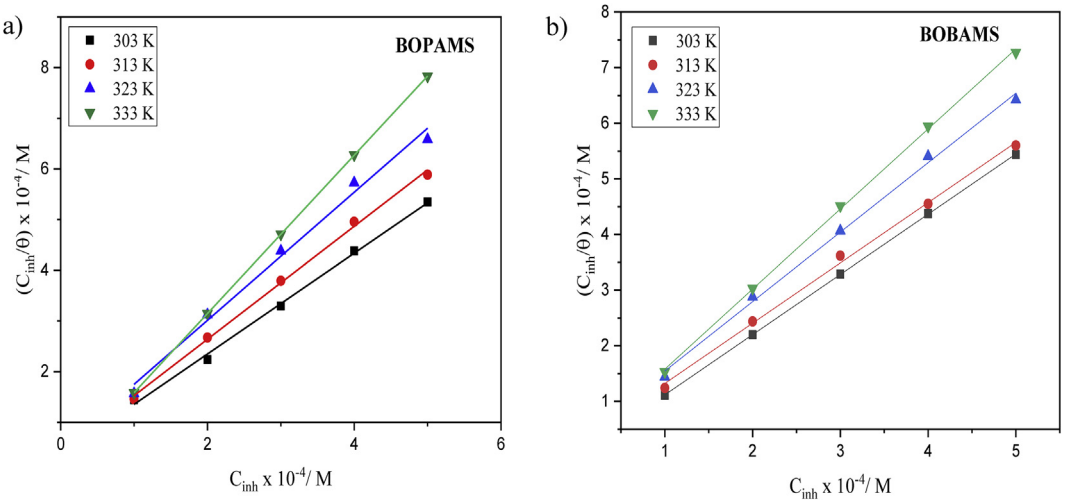

Figure 9. Langmuir isotherms of Al utilizing 1M HCl for the process without and with of various molarities of a) BOPAMS and b) BOBAMS at various temperatures.

where the numeral 55.5 represent the molarity of H_2O in solution, ΔG°_{ads} represents the standard Gibb's free energy of the binding process, R represents the universal gas constant and T is the absolute temperature.

Figure 9 represents the relation between C_{inh}/θ versus C_{inh} which gave straight lines for the two inhibitors with a slope approximately equal to unity and non-zero intercepts at all temperatures investigated. For example, the linear correlation coefficient (R^2) for BOPAMS are 0.9966, 0.9974, 0.9957 and 1 at 303K, 313K, 323K and 333K, respectively. This confirms that the adsorption layer formed by the three inhibitors on the Al surface in 1M HCl obeys the Langmuir adsorption

Table 6. Thermodynamic and adsorption data of Al corrosion utilizing 1M HCl for the process at various temperatures for BOPAMS and BOBAMS.

Inhibitor	T/K	R^2	Slope	K_{ads}/L.mol^{-1}	$-\Delta G^{\circ}_{ads}$/kJ.mol^{-1}	ΔH°_{ads}/kJ. mol^{-1}	ΔS°_{ads}/J.mol^{-1}.K^{-1}
BOPAMS	303	0.9966	0.9942	2779.2	30.0962		324
	313	0.9974	1.1141	2432.1	30.7423	68*	315
	323	0.9957	1.2634	2055.9	31.2732	68**	307
	333	1.0000	1.5621	44306.6	40.7426		327
BOBAMS	303	0.9999	1.0825	28264.6	35.9396	– 36*	– 0.2
	313	0.9968	1.0835	4174.5	32.1483	– 36**	– 12
	323	0.9962	1.2487	3365.1	32.5965		– 11
	333	0.9992	1.4394	7095.2	35.6711		– 0.99

* Parameters obtained utilizing Van't Hoff expression.
** Parameters derived from the Gibbs-Helmholtz expression.

isotherm. The closeness of the slope to unity also indicates that the type of the adsorption layer formed on the Al surface is a monolayer (Ogunleye et al., 2020).

The data of ΔG°_{ads} ranging up to –20 kJ mol^{-1} are generally associated with some electrostatic interaction taking place around the charged metal surface and BOPAMS and BOBAMS (physical adsorption) while the data around –40 kJ mol^{-1} and beyond are associated with the exchange of electrons between Al and BOPAMS and BOBAMS resulting in the formation of a strong chemical bond (chemical adsorption) (El-Lateef et al., 2019; Lgaz et al., 2016). In this work, the ΔG°_{ads} data for BOBAMS and BOPAMS were all above –20 kJ mol^{-1} yet slightly below –40 kJ mol^{-1}, signifying mixed-type binding process on Al surface, with a dominating chemisorption mechanism as the values are nearing the –40 kJ mol^{-1} value. The data of ΔG^{o}_{ads} showed similar behaviour to those for K_{ads} as they seem to increase with a temperature rise. This implies some change in the adsorption mechanism from a physical to a chemical type of adsorption. (–) data of ΔG°_{ads} support the spontaneous type of binding process.

Thermodynamic properties like the enthalpy of adsorption ΔH°_{ads} and ΔS°_{ads} can be utilized to further understand the binding process of BOPAMS and BOBAMS on Al surface. ΔH°_{ads} data may be deduced by utilizing the Van't Hoff expression (7) (Tang et al., 2003).

$$lnK = -\frac{H^{\circ}_{ads}}{RT} + constant \tag{7}$$

where K represents the adsorption equilibrium constant, R represents the universal gas constant and T represents the absolute temperature.

Gibbs-Helmholtz expression may also be utilized to obtain the enthalpy of adsorption (Noor, 2007).

$$\left[\frac{\partial\left(\Delta G^{\circ}_{ads}/T\right)}{\partial T}\right]_P = -\frac{\Delta H^{\circ}_{ads}}{T^2} \tag{8}$$

Gibbs-Helmholtz expression (8) may also be rearranged to give expression in Eq. (9).

$$\frac{\Delta G^{\circ}_{ads}}{T} = \frac{H^{\circ}_{ads}}{T} + k \tag{9}$$

ΔS°_{ads} can be calculated from ΔG°_{ads} and ΔH°_{ads} as shown in Eq. (10).

$$\Delta S^{\circ}_{ads} = \frac{\Delta H^{\circ}_{ads} - \Delta G^{\circ}_{ads}}{T} \tag{10}$$

Table 6 reports the data of ΔH^{o}_{ads} and ΔS^{o}_{ads} over the temperature range of 303–313K. It has been reported in literature (Amin et al., 2007; Al-Amiery et al., 2013) that if $\Delta H^{o}_{ads} > 0$ (endothermic), then the inhibitors adsorb chemically on the metal surface, and if $\Delta H^{o}_{ads} < 0$ (exothermic), then the adsorption process can either be taking place through chemisorption or physisorption process. In cases where the $\Delta H^{o}_{ads} < 0$, physisorption process can be differentiated from chemisorption based on the magnitude of ΔH^{o}_{ads}. To classify the adsorption as physisorption, the ΔH^{o}_{ads} data is normally less than 40 kJ mol^{-1} and it is greater than 100 kJ mol^{-1} for chemisorption (Zarrouk et al., 2011). For BOPAMS, the ΔH^{o}_{ads} values are higher than 40 kJ mol^{-1} yet lower than 100 kJ mol^{-1} showing that the binding process is both of physisorption and chemisorption nature. Additionally, (+) values of ΔS^{o}_{ads} with the addition of BOPAMS signifies a rise in the entropy of the solvent. This means that there is a disorder occurring on the metal surface because of the molecules of H_2O which gets detached from the Al surface. In the case where the ΔS^{o}_{ads} values are (+). Literature says that the fall of enthalpy may be the chief motive for the binding of BOPAMS molecules on Al

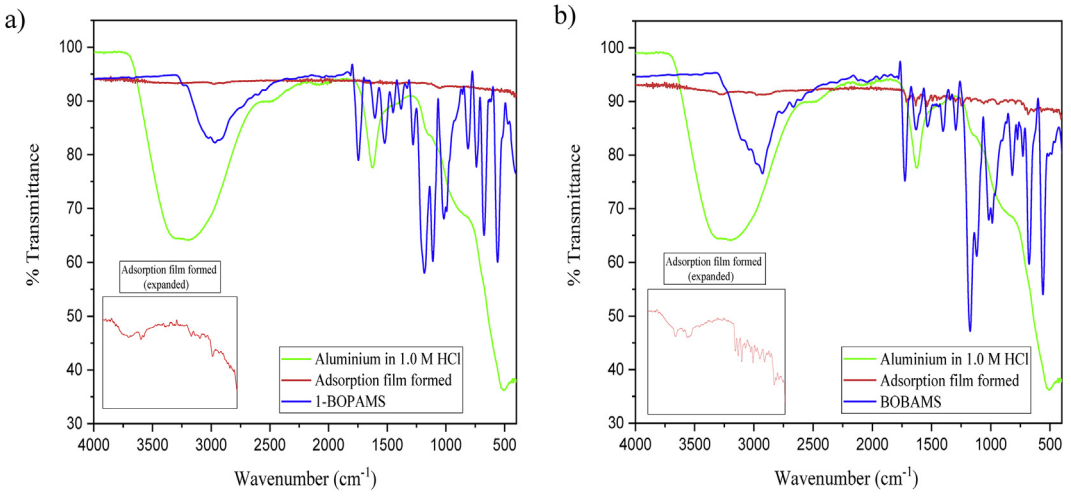

Figure 10. FT-IR spectra comparison of the frequencies for the pure compound and adsorption films resulted on the Al in 1.0 M HCl by a) BOPAMS and b) BOBAMS.

(Avci, 2008). For BOBAMS, ΔH^{o}_{ads} values are –36 kJ mol^{-1}, and this is indicative of dominating physical adsorption process. (–) ΔS°_{ads} values for BOBAMS suggest that the binding process is of an exothermic nature. For this instance, the BOPAMS and BOBAMS molecules are said to first move into the solution before binding on the Al surface and they do so in some arranged pattern onto the surface of Al, and consequently bring about a fall in entropy (Li and Mu, 2005; Li et al., 2010). The adsorption process being exothermic, thermodynamic principle indicates that it must be accompanied by a reduction in entropy (Mu et al., 2005).

3.6. Adsorption film analysis

FT-IR instrument was utilized to analyze the characteristics associated with the protective film that resulted on the surface of Al. FT-IR spectra of Al submerged in aggressive HCl without and with of BOPAMS and BOBAMS (adsorption film formed) were compared to the spectra of the two pure synthesized compounds as shown in Figure 10. The inspection of the spectra of Al in aggressive HCl without the BOPAMS and BOBAMS show a broad peak around 3261.62 cm^{-1} and a weak peak around 1624.44 cm^{-1} which is indicative of the presence of hydrated aluminium oxide molecule ($Al_2O_3.xH_2O$) and the presence of water. The stretching frequency of around 849.75 and 502 cm^{-1} represents the γ-AlO_4 and γ-AlO_6, respectively. Thus, the γ-Al_2O_3 phase contained both octahedral and tetrahedral coordination (Potdar et al., 2007). The expanded adsorption film formed spectra for BOBAMS and BOPAMS are drawn to highlight the fact that the intensity of the peaks decreased to the point that they look as if they have disappeared due to the smaller scale. This indicates some high strength interaction taking place in the midst the functional groups of the two compounds and Al. These include the ammonium salt ($^{+}NH_3$), O=S=O, S–O^{-}, C–N and C–O, which are some possible electron donors. The disappearance of the peaks can be attributed to the resultant strong Al–BOBAMS or Al–BOPAMS and the reason for the high inhibition efficiencies exhibited by BOBAMS and BOPAMS.

3.7. Proposed inhibition mechanism between Al and BOPAMS/BOBAMS

The inhibition capabilities related to inhibitor molecules for Al corrosion are said to be a result of the binding of BOPAMS/BOBAMS molecules on Al, resulting in a protective barrier. The degree of binding offered by the inhibitors is highly dependent on factors such as the condition of the surface of the metal, type of the metal and the mechanism of binding of the inhibitor molecules (Curkovic et al., 2010). During the inhibition process in aggressive HCl solution, the binding of inhibitor molecules at the Al/OH^{-} boundary is assumed to be the initial step. The adsorption may be because of one of three steps, namely; an electrostatic attraction that occurs between charged Al surface and charged BOPAMS/BOBAMS, the formation of coordination bond by the unshared pair of electrons on the BOPAMS/BOBAMS and the empty or half-filled p-orbitals from the Al atoms and the participation of the π-electrons of the BOPAMS/BOBAMS (Schweinsberg et al., 1988; El-Rehim et al., 1999). As such, the prevention of Al corrosion in HCl is accomplished largely as a result of electrostatic interaction; this conclusion is supported by the fall in the %IE with the rise in absolute T. Generally, the inhibitors can be adsorbed on the Al surface either in their neutral or protonated forms. In acidic solution (i.e., HCl), the Al surface is negatively charged and as a result, protonated IL molecules find it easier to attack the negatively charged surface as a result of electrostatic attraction that occurs between them and the Al surface (Desai, 1972). The binding of BOPAMS/BOBAMS is said to involve the replacement of the H_2O molecules on the surface of Al and the exchange of electrons that occurs in the midst of the Al surface and heteroatoms of BOPAMS/BOBAMS.

4. Conclusions

- BOPAMS and BOBAMS are mixed-type anti-corrosive substances for Al in aggressive acid environment solution and obeys Langmuir adsorption isotherm. The highest IE% obtained for BOPAMS and BOBAMS are 97.57% and 97.84%, respectively.
- Polarization study revealed that BOPAMS and BOBAMS act in both oxidation and reduction half-reactions for Al with the reduction half-reaction being polarized more. From the polarization study corrosion parameters E_{corr}, I_{corr}, β_a and β_c were obtained. These parameters indicated that BOPAMS and BOBAMS are mixed type corrosion inhibitors and the inhibition of Al was mainly controlled by charge transfer. The increase of the R_P values with an increase in the concentration of the inhibitors indicated that the inhibition of corrosion is primarily due to the formation of the protective film.
- The inhibition efficiencies of BOPAMS and BOBAMS increased with improving their concentrations and fell with the rise of the temperature.
- Al showed Nyquist plots with a more pronounced passive region, and this is attributed to the higher tendency of Al in forming an oxide film. EIS results showed that the charge transfer resistance increased as the concentration of the inhibitors were increased leading to the decrease of the corrosion rate and higher %IE. The constant phase element exponent (n) values were near unity for Al which is indicative of a pseudo-capacitive behaviour of the electrode. Mixed-type adsorption was exhibited for the two inhibitors studied.

Declarations

Author contribution statement

Tshimangadzo Nesane: Performed the experiments; Analyzed and interpreted the data; Wrote the paper.

Simon S. Mnyakeni-Moleele: Conceived and designed the experiments; Analyzed and interpreted the data; Wrote the paper.

Lutendo C. Murulana: Conceived and designed the experiments; Contributed reagents, materials, analysis tools or data; Wrote the paper.

Funding statement

This work was supported by the South African National Research Foundation (NRF) Thuthuka (grant 107341) and the South African Synthetic Oil Limited (SASOL) University Collaboration Programme Grant.

Competing interest statement

The authors declare no conflict of interest.

Additional information

No additional information is available for this paper.

Acknowledgements

The authors acknowledge South African National Research Foundation (NRF) and South African Synthetic Oil Limited (SASOL).

References

Abdulwahab, M., Oladijo, O.E., Loto, C.O., Oladijo, O.P., 2016. Corrosion resistance of AA2036 and AA7075–T651 in contaminated acid chloride environments. Asian J. Chem. 28, 1453–1462.

Al-Amiery, A.A., Kadhum, A.A.H., Mohamad, A.B., Musa, A.Y., Li, C.J., 2013. Electrochemical study on newly synthesized chlorocurcumin as an inhibitor for mild steel corrosion in hydrochloric acid. Materials 6, 5466–5477.

Alaoui, K., El Kacimi, Y., Galai, M., Serrar, H., Touir, R., Kaya, S., Kaya, C., Ebn Touhami, M., 2020. New triazepine carboxylate derivatives: correlation between corrosion inhibition property and chemical structure. Int. J. Ind. Chem. 11, 23–42.

Amin, M.A., El-Rehim, S.S.A., El-Sherbini, E.E.F., Bayoumi, R.S., 2007. The inhibition of low carbon steel corrosion in hydrochloric acid solutions by succinic acid part I. Weight loss, polarization, EIS, PZC, EDX and SEM studies. Electrochim. Acta 52, 3588–3600.

Antonijevic, M.M., Petrovic, M.B., 2008. Copper corrosion inhibitors-A review. Int. J. Electrochem. Sci. 3, 1–28.
Atta, A.M., El-Mahdy, G.A., Al-Lohedan, H.A., Ezzat, A.R.O., 2015. A new green ionic liquid-based corrosion inhibitor for steel in acidic environments. Molecules 20, 11131–11153.
Avci, G., 2008. Corrosion inhibition of indole-3-acetic acid on mild steel in 0.5 M HCl. Colloid. Surface. Physicochem. Eng. Aspect. 317, 730–736.
Curkovic, H.O., Stupnisek-Lisac, E., Takenouti, H., 2010. The influence of pH value on the efficiency of imidazole based corrosion inhibitors of copper. Corrosion Sci. 52, 398–405.
Desai, M., 1972. Corrosion inhibitors for aluminium alloys. Mater. Corros. 23, 475–482.
Ekanem, U.F., Umoren, S.A., Udousoro, I.I., Udoh, A.P., 2010. Inhibition of mild steel corrosion in HCl using pineapple leaves (Ananas comosus L.) extract. J. Mater. Sci. 45, 5558–5566.
El-Azaly, A.M., 2019. Influence of Soybean (Glycine Max) plant extract on corrosion of aluminum in 1M HCl. Int. J. Electrochem. Sci. 14, 2714–2731.
El-Katori, E.E., Fouda, A.S., Mohamed, R.R., 2020. Synergistic corrosion inhibition activity of the chicoriumintybus extract and iodide ions for mild steel in acidic media. J. Chil. Chem. Soc. 65, 4672–4681.
El-Lateef, H.M.A., Abdel-Rahman, E.S., Mohran, H.S., Shilkamy, H.A.S., 2019. Corrosion inhibition and adsorption behavior of phytic acid on Pb and Pb–In alloy surfaces in acidic chloride solution. Int. J. Ind. Chem. 10, 31–47.
El-Rehim, S.A., Ibrahim, M.A., Khaled, K.F., 1999. 4-Aminoantipyrine as an inhibitor of mild steel corrosion in HCl solution. J. Appl. Electrochem. 29, 593–599.
El-Shamy, A.M., Zakaria, K., Abbas, M.A., El Abedin, S.Z., 2015. Anti-bacterial and anti-corrosion effects of the ionic liquid 1-butyl-1-methylpyrrolidinium trifluoromethylsulfonate. J. Mol. Liq. 211, 363–369.
Ezeoke, A.U., Adeyemi, O.G., Akerele, O.A., Obi-Egbedi, N.O., 2012. Computational and experimental studies of 4-aminoantipyrine as corrosion inhibitor for mild steel in sulphuric acid solution. Int. J. Electrochem. Sci. 7, 534–553.
Ghames, A., Douadi, T., Issaadi, S., Sibous, L., Alaoui, K.I., Taleb, M., Chafaa, S., 2017. Theoretical and experimental studies of adsorption characteristics of newly synthesized schiff bases and their evaluation as corrosion inhibitors for mild steel in 1 M HCl. Int. J. Electrochem. Sci. 12, 4867–4897.
Govindasamy, R., Ayappan, S., 2015. Study of Corrosion inhibition properties of novel Semicarbazones on mild steel in acidic solutions. J. Chil. Chem. Soc. 60, 2786–2798.
Hachelef, H., Benmoussat, A., Khelifa, A., Athmani, D., Bouchareb, D., 2016. Study of corrosion inhibition by electrochemical impedance spectroscopy method of 5083 aluminum alloy in 1 M HCl solution containing propolis extract. J. Mater. Environ. Sci. 7, 1751–1758.
Kciuk, M., Tkaczyk, S., 2007. Structure, mechanical properties and corrosion resistance of AlMg5 and AlMg1Si1 alloys. J. Achiev. Mater. Manuf. Eng. 21, 39–42.
Kciuk, M., Kurc, A., Szewczenko, J., 2010. Structure and corrosion resistance of aluminium AlMg2. 5; AlMg5Mn and AlZn5Mg1 alloys. J. Achiev. Mater. Manuf. Eng. 41, 74–81.
Khaled, K.F., Al-Qahtani, M.M., 2009. The inhibitive effect of some tetrazole derivatives towards Al corrosion in acid solution: chemical, electrochemical and theoretical studies. Mater. Chem. Phys. 113, 150–158.
Kim, D.K., Muralidharan, S., Ha, T.H., Bae, J.H., Ha, Y.C., Lee, H.G., Scantlebury, J.D., 2006. Electrochemical studies on the alternating current corrosion of mild steel under cathodic protection condition in marine environments. Electrochim. Acta 51, 5259–5267.
Ladha, D.G., Wadhwani, P.M., Kumar, S., Shah, N.K., 2015. Evaluation of corrosion inhibitive properties of trigonellafoenum-graecum for pure aluminium in hydrochloric acid. J. Mater. Environ. Sci. 6, 1200–1209.
Lgaz, H., Salghi, R., Larouj, M., Elfaydy, M., Jodeh, S., Rouifi, Z., Lakhrissi, B., Oudda, H., 2016. Experimental, theoretical and Monte Carlo simulation of quinoline derivative as effective corrosion inhibitor for mild steel in 1 M HCl. J. Mater. Environ. Sci. 7, 4471–4488.
Li, X., Mu, G., 2005. Tween-40 as corrosion inhibitor for cold rolled steel in sulphuric acid: weight loss study, electrochemical characterization, and AFM. Appl. Surf. Sci. 252, 1254–1265.
Li, X., Deng, S., Fu, H., 2010. Adsorption and inhibition effect of vanillin on cold rolled steel in 3.0 M H_3PO_4. Prog. Org. Coating 67, 420–426.
Maayt, A.K., Al-Rawashdeh, N.A.F., 2004. Inhibition of acidic corrosion of pure aluminum by some organic compounds. Corrosion Sci. 46, 1129–1140.
Mu, G., Li, X., Liu, G., 2005. Synergistic inhibition between tween 60 and NaCl on the corrosion of cold rolled steel in 0.5 M sulfuric acid. Corrosion Sci. 47, 1932–1952.
Murulana, L.C., Kabanda, M.M., Ebenso, E.E., 2015. Experimental and theoretical studies on the corrosion inhibition of mild steel by some sulphonamides in aqueous HCl. RSC Adv. 5, 28743–28761.
Musa, A.Y., Kadhum, A.A.H., Mohamad, A.B., Takriff, M.S., 2010. Experimental and theoretical study on the inhibition performance of triazole compounds for mild steel corrosion. Corrosion Sci. 52, 3331–3340.
Nessim, M.I., Zaky, M.T., Deyab, M.A., 2018. Three new gemini ionic liquids: synthesis, characterizations and anticorrosion applications. J. Mol. Liq. 266, 703–710.
Noor, E.A., 2007. Temperature effects on the corrosion inhibition of mild steel in acidic solutions by aqueous extract of fenugreek leaves. Int. J. Electrochem. 2, 996–1017.
Ogunleye, O.O., Arinkoola, A.O., Eletta, O.A., Agbede, O.O., Osho, Y.A., Morakinyo, A.F., Hamed, J.O., 2020. Green corrosion inhibition and adsorption characteristics of Luffa cylindrica leaf extract on mild steel in hydrochloric acid environment. Heliyon 6, e03205.
Potdar, H.S., Jun, K.W., Bae, J.W., Kim, S.M., Lee, Y.J., 2007. Synthesis of nano-sized porous γ-alumina powder via a precipitation/digestion route. Appl. Catal. A-Gen. 321, 109–116.
Qiang, Y., Zhang, S., Guo, L., Zheng, X., Xiang, B., Chen, S., 2017. Experimental and theoretical studies of four allyl imidazolium-based ionic liquids as green inhibitors for copper corrosion in sulfuric acid. Corrosion Sci. 119, 68–78.
Schweinsberg, D.P., George, G.A., Nanayakkara, A.K., Steinert, D.A., 1998. The protective action of epoxy resins and curing agents-inhibitive effects on the aqueous acid corrosion of iron and steel. Corrosion Sci. 28, 33–42.
Shalabi, K., Abdallah, Y.M., Fouda, A.S., 2015. Corrosion inhibition of aluminum in 0.5 M HCl solutions containing phenyl sulfonylacetophenoneazo derivatives. Res. Chem. Intermed. 41, 4687–4711.
Subasri, R., Shinohara, T., Mori, K., 2005. Modified TiO_2 coatings for cathodic protection applications. Sci. Technol. Adv. Mater. 6, 501–507.
Tang, L., Mu, G., Liu, G., 2003. The effect of neutral red on the corrosion inhibition of cold rolled steel in 1.0 M hydrochloric acid. Corrosion Sci. 45, 2251–2262.
Tsuru, T., Haruyama, S., Gijutsu, B., 1978. Corrosion inhibition of iron by amphoteric surfactants in 2 M HCl. Jpn. Soc. Corros. Eng. 27, 573–581.
Uhlig, H.H., King, C., 1972. Corrosion and corrosion control. J. Electrochem. Soc. 119, 327.
Umoren, S., 2009. Polymers as corrosion inhibitors for metals in different media-A review. Open Corrosion J. 2, 175–188.
Verma, C., Singh, P., Bahadur, I., Ebenso, E.E., Quraishi, M.A., 2015. Electrochemical, thermodynamic, surface and theoretical investigation of 2-aminobenzene-1, 3-dicarbonitriles as green corrosion inhibitor for aluminum in 0.5 M NaOH. J. Mol. Liq. 209, 767–778.
Verma, C., Obot, I.B., Bahadur, I., Sherif, E.M., Ebenso, E.E., 2018. Choline based ionic liquids as sustainable corrosion inhibitors on mild steel surface in acidic medium: gravimetric, electrochemical, surface morphology, DFT and Monte Carlo simulation studies. Appl. Surf. 457, 134–149.
Verma, C., Saji, V.S., Quraishi, M.A., Ebenso, E.E., 2020. Pyrazole derivatives as environmental benign acid corrosion inhibitors for mild steel: experimental and computational studies. J. Mol. Liq. 298, 111943.
Yurt, A., Ulutas, S., Dal, H., 2006. Electrochemical and theoretical investigation on the corrosion of aluminium in acidic solution containing some Schiff bases. Appl. Surf. 253, 919–925.
Zarrouk, A., Hammouti, B., Zarrok, H., Al-Deyab, S.S., Messali, M., 2011. Temperature effect, activation energies and thermodynamic adsorption studies of L-cysteine methyl ester hydrochloride as copper corrosion inhibitor in nitric acid 2M. Int. J. Electrochem. Sci. 6, 6261–6274.
Zhang, H.H., Zhang, Y., Yang, Z.N., 2014a. Investigation of 4-methoxysalicylaldehyde thiosemicarbazone as inhibitor for carbon steel in sulfuric acid solution. Appl. Mech. Mater. 633, 513–516.
Zheng, X., Zhang, S., Gong, M., Li, W., 2014b. Experimental and theoretical study on the corrosion inhibition of mild steel by 1-octyl-3-methylimidazolium L-prolinate in sulfuric acid solution. Ind. Eng. Chem. Res. 53, 16349–16358.